Permeation of Phospholipid Membranes by Peroxynitrite[†]

Rafail F. Khairutdinov, John W. Coddington, and James K. Hurst*

Department of Chemistry, Washington State University, Pullman, Washington 99164-4630

Received June 2, 2000; Revised Manuscript Received September 18, 2000

ABSTRACT: Quantitative kinetic models have been developed for the reaction between peroxynitrite and membrane lipids in vesicles and for transmembrane oxidation of reactants located within their inner aqueous cores. The models were used to analyze TBARS formation and oxidation of entrapped $Fe(CN)_6^{4-}$ ion in egg lecithin liposomes and several artificial vesicles. The analyses indicate that permeation of the bilayers by ONOOH and $NO_2^{\bullet}$, a radical formed by homolysis of the ONOOH bond, is unusually rapid but that permeation by $ONOO^-$ and $CO_3^{\bullet-}$, a radical formed when CO_2 is present, is negligible. Bicarbonate protects the vesicles against both membrane and $Fe(CN)_6^{4-}$ oxidation by rapid competitive CO_2-catalyzed isomerization of ONOOH to NO_3^-; this effect is partially reversed by addition of nitrite ion, which reacts with $CO_3^{\bullet-}$ to generate additional $NO_2^{\bullet}$. Under medium conditions mimicking the physiological milieu, a significant fraction of the oxidants escape to inflict damage upon the vesicular assemblies. Rate constants for several elementary reaction steps, including transmembrane diffusion rates for ONOOH and $NO_2^{\bullet}$, were estimated from the bicarbonate dependence of the oxidative reactions.

The biochemical reactions of peroxynitrous acid (ONOOH)[1] and related reactive nitrogen species have been suggested to represent a new paradigm for oxidative stress (*1*−*3*). The conjugate base of this powerful oxidant (*4*), i.e., $ONOO^-$ ($pK_a = 6.6$), is thought to be generated by radical combination of the superoxide anion ($O_2^{\bullet-}$) and nitric oxide ($NO^{\bullet}$) (*5*) in biological environments where these are simultaneously formed, including phagocytes, neuronal tissues, and the blood stream. The bulk of $ONOO^-$ that is not scavenged by physiological antioxidants (*1*, *6*−*8*) is thought to react with CO_2 (*6*, *8*) to form the transient adduct, nitrosoperoxycarbonate ($ONOOCO_2^-$). This species has not been isolated because its rate of decomposition exceeds its rate of formation; its composition is dictated by the kinetic rate law, which is first-order in both $ONOO^-$ and CO_2 (*9*−*11*). Ab initio calculations indicate that geometrical structures similar to those for ONOOH, with CO_2 replacing H^+ as the Lewis acid, are energetically stable (*12*). However, the calculated peroxo O−O bond dissociation energy in $ONOOCO_2^-$ is extremely weak (∼9 kcal/mol, compared to ∼52 kcal/mol for HOOH). As a consequence, many chemical oxidations by $ONOOCO_2^-$ appear to be sequential, involving prior O−O bond homolysis to form the radicals $NO_2^{\bullet}$ and $CO_3^{\bullet-}$, which then engage in one-electron oxidations of reacting partners (*13*, *14*). Indeed, the carbonate radical has recently been shown by flow-EPR experiments to form in quantities predicted by this radical mechanism during reaction between $ONOO^-$ and CO_2 (*15*). Although the mechanism of decomposition of ONOOH has been controversial (*4*, *16*−*18*), recent kinetic studies have provided strong evidence for an analogous mechanism involving O−O bond homolysis to form $NO_2^{\bullet}$ and $OH^{\bullet}$ (*19*−*23*).

A critical issue has emerged concerning the putative role of these short-lived radicals in injury to tissues, namely, whether they have sufficient lifetimes in physiological environments to diffuse to cellular target sites and cause significant oxidative damage. As an illustrative example, consider the toxicity of ONOOH and $CO_3^{\bullet-}$ toward aqueous suspensions of *Escherichia coli*. Both ONOOH (*24*−*26*) and radiolytically generated $CO_3^{\bullet-}$ (*27*) are highly toxic to the bacteria. Although both oxidation rates and product yields of many reactions between peroxynitrite and chemical reductants are increased in bicarbonate-containing media by intermediary formation of $ONOOCO_2^-$ (*28*), bicarbonate buffers completely protect the bacteria from killing by peroxynitrite (*24*, *26*). Similar protection by bicarbonate has been observed in peroxynitrite killing of the parasite *Trypanosoma cruzi* (*29*). The difference in radiolytically generated and chemically generated $CO_3^{\bullet-}$ (i.e., from $ONOOCO_2^-$) appears to be that, in the latter case, $NO_2^{\bullet}$ is also formed and can undergo radical recombination to give CO_2 and NO_3^- as benign products. Carbon dioxide thereby catalyzes ONOOH decomposition (*14*, *30*), dramatically shortening its lifetime. When the characteristic diffusion length becomes shorter than the distance to the target site, the oxidant will no longer be an effective toxin. In general, it is an open question of whether $ONOOCO_2^-$ formation serves to protect cells from damage by peroxynitrite or promotes damage by substituting the more selective oxidant $CO_3^{\bullet-}$ for $OH^{\bullet}$ (*6*).

[†] Financial support was provided by the National Institutes of Health via Grant AI-15834.

* To whom correspondence should be addressed.

[1] Abbreviations: ONOOH, peroxynitrous acid, also called peroxonitrous acid or pernitrous acid (IUPAC name, hydrogen oxoperoxonitrate); $ONOOCO_2^-$, nitrosoperoxycarbonate, also called nitrosoperoxycarboxylate (IUPAC name, 1-carboxylato-2-nitrosodioxidane); DMPC, dimyristoylphosphatidylcholine; DPPC, dipalmitoylphosphatidylcholine; MDA, malondialdehyde; PAPC, β-arachidonoyl-γ-palmitoylphosphatidylcholine; PC, phosphatidylcholine; TBARS, thiobarbituric acid-reactive substances.

10.1021/bi001270x CCC: $19.00
Published on Web 10/24/2000

One important aspect of this general question of intrinsic reactivity versus diffusion lengths is the mobility of peroxynitrite within tissues. In 25 mM bicarbonate at pH 7.4 and 37 °C, the mean lifetime of ONOOH is 10−20 ms (*31*), so (from Einstein's diffusion equation, $\overline{L^2} = 6Dt$, where the coefficient 6 reflects the mean-square displacement in three dimensions) the average distance traversed by ONOOH before undergoing CO_2-catalyzed decomposition, if unhindered, would be ∼12 μm, several times the mean diameter of erythrocytes and leukocytes. Thus, questions concerning the inter- and intracellular accessibility of peroxynitrite-based oxidants depend critically upon the extent to which ONOOH and $ONOO^-$ can cross biological membranes. Peroxynitrite permeabilities have been examined by several groups using both phospholipid-based model membranes and erythrocytes without a clear consensus having been reached. Using a commercially available artificial liposome kit containing egg phosphatidylcholine (PC), cholesterol, and stearylamine to prepare large unilamellar vesicles containing a water-soluble cationic Mn(III) porphyrin derivative as the reductant, Groves and co-workers (*32*) found that the membrane bilayer presented no significant barrier to peroxynitrite diffusion and calculated an apparent permeability coefficient (*P*) which was only a factor of 3 less than that of water. They also reported that the presence of CO_2 did not significantly inhibit the amount of peroxynitrite crossing the bilayer and that the extent of transmembrane diffusion was pH-independent over the pH range of 7.4−8.2, implying that a facile pathway existed for translocation of the $ONOO^-$ anion. Work by Radi and co-workers (*8*, *31*) on transmembrane oxidation of oxyhemoglobin in erythrocytes by peroxynitrite, while not yielding a value for *P*, also indicated that the erythrocyte membrane did not constitute a significant barrier to ONOOH but that permeation by $ONOO^-$ occurred primarily, if not exclusively, through the membrane-localized band 3 anion exchange protein. In their system, intracellular oxidation of oxyhemoglobin was extensively inhibited by CO_2. Nitration of a tyrosine-substituted SOD mutant entrapped within erythrocyte ghosts has been investigated by Beckman and co-workers (*33*). At pH 7.5, nitration was inhibited by 90% when the band 3 anion exchange protein was inhibited with phenyl isothiocyanate, suggesting that nearly all of the peroxynitrite permeated via the anion channel and, by inference, that passive transmembrane diffusion of ONOOH across the bilayer is not particularly rapid.

Although some of these results appear contradictory, it must be recognized that the reaction dynamics of this system are complex (see, for example, Figure 1), involving extracellular decomposition of the oxidant at rates that are highly dependent upon the medium conditions in addition to intracellular trapping by redox reagents that react by complex rate laws. To develop useful kinetic models that describe accurately the dynamics of these types of systems and to gain quantitative understanding of the diffusional behavior of ONOOH, we have examined both the membrane lipid oxidation and transmembrane oxidation of the $Fe(CN)_6^{4-}$ ion occluded within artificial and egg PC liposomes by peroxynitrite added to the extracellular medium. From the dependence of yields of oxidized product upon the CO_2 content of the medium, it has been possible to determine the permeability of peroxynitrite. The value obtained for the permeability coefficient was nearly identical to that reported by Groves and co-workers (*32*) and several 100-fold greater than permeability coefficients reported for other polar nonelectrolytes (*34*). This unusally high permeability can be rationalized, at least in part, by recognizing that $NO_2^•$ is also a membrane-permeable oxidant.

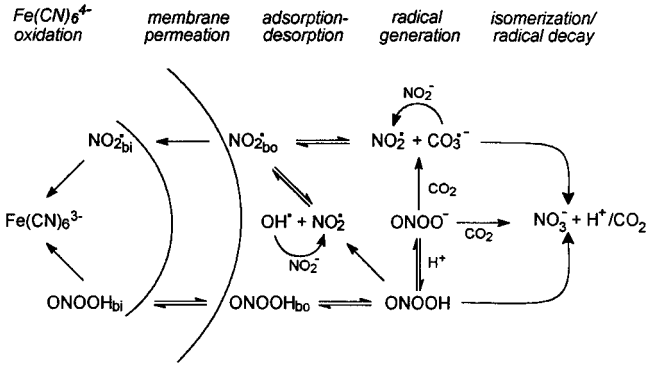

FIGURE 1: Minimal reaction scheme showing the major pathways for intravesicular $Fe(CN)_6^{4-}$ oxidation by externally added peroxynitrite in the presence of bicarbonate. Reactions involving formation, decay, and transmembrane diffusion of N_2O_4 (reactions 7−9, 15c, and 16c) are not shown for the sake of clarity. Note also that the caged radical pairs $\{NO_2^•,OH^•\}$ and $\{NO_2^•,CO_3^{•-}\}$, which are common intermediates in the isomerization and radical-generating reactions of ONOOH (*20*) and $ONOOCO_2^-$ (*9*), respectively, have not been shown.

EXPERIMENTAL PROCEDURES

Preparation of Reactants. Egg phosphatidylcholine was isolated by solvent extraction and chromatography on alumina (*35*); the purified product was stored at −10 °C as a chloroform solution. Unilamellar vesicles were prepared by rotary evaporation of portions of the stock solutions in round-bottom flasks to form dry films, hydration of the PC by suspension in an appropriate aqueous buffer followed by several freeze−thaw cycles, and then repeated high-pressure extrusion with N_2 gas through 0.5 μm porosity track-etched filters (*36*). Prepared in this way, the vesicles had a relatively narrow size distribution with an external diameter of ∼70 nm (*36*). Vesicles made from commercial dipalmitoylphosphatidylcholine (DPPC) and dimyristoylphosphatidylcholine (DMPC), including those doped with small amounts of β-arachidonoyl-γ-palmitoylphosphatidylcholine (PAPC), were similarly prepared, except that the temperature during extrusion was maintained at ∼10 °C above that for the surfactant gel−liquid transition (42 °C for DPPC and 24 °C for DMPC). Vesicles containing entrapped potassium ferrocyanide were prepared by forming them in buffers containing 0.2−0.3 M $Fe(CN)_6^{4-}$, followed by removing external ferrocyanide by size exclusion chromatography on Sephadex G-100. Typically, 10 mL of the vesicle preparation was applied to a 30 cm × 2 cm column and collected in an equal volume of eluate following passage of the void volume. The amount of entrapped $Fe(CN)_6^{4-}$ was determined by destroying the vesicles by addition of an equal volume of acetonitrile, centrifugation to remove precipitated phospholipid, oxidation of the complex ion in the supernatant to $Fe(CN)_6^{3-}$, and determination of its concentration by spectrophotometric analysis using an ϵ_{420} of 1.1×10^3 M^{-1} cm^{-1}. A reagent solution of sodium peroxynitrite was prepared by flow-

mixing acidic solutions of hydrogen peroxide and sodium nitrite, followed by rapid quenching with sodium hydroxide (*37*), and was stored at −80 °C. The peroxynitrite concentration was determined to be 140 mM by spectrometric analysis using an ϵ_{302} of 1670 M^{-1} cm^{-1} (*38*); these solutions also contained 15% (21 mM) nitrite ion, as determined by the Griess method (*39*).

Chemical Reactions. Generally, the vesicle suspensions were deoxygenated by bubbling gently with argon for 20−60 min prior to reacting them with peroxynitrite. However, the presence of O_2 did not appear to significantly affect the results. For reaction, 0.7 mL portions of the vesicles were transferred to small plastic Eppendorf centrifuge tubes, and a small amount of suitably diluted peroxynitrite solution (e.g., 7.5 μL of a 46 mM solution) was introduced as an adherent droplet attached to the tube wall above the vesicle solution. After the vial had been capped, the reaction was initiated by rapid vortex mixing. To examine the CO_2 dependence of the reaction, a small amount of concentrated bicarbonate buffer was added to the preformed vesicle suspension and incubated for a few minutes prior to addition of the peroxynitrite to allow equilibration across the bilayer membrane. The extent of oxidation of $Fe(CN)_6^{4-}$ was determined spectrophotometrically from the increase in absorbance at 420 nm, the absorption maximum for $Fe(CN)_6^{3-}$. Oxidation rates, as well as rates of decomposition of ONOOH and the bimolecular reaction of $ONOO^-$ with CO_2, were monitored using a Hi-Tech SF-40 stopped-flow instrument. Oxidative damage to membrane lipids was assessed by spectrophotometric determination of the amount of thiobarbituric acid-reactive substances (TBARS) formed using a simplified version of a standard protocol (*40*). Specifically, because the light scattering from the samples was negligible at 532 nm, it was possible to measure directly the malondialdehyde (MDA) concentration without extracting it from the reaction medium. Oxidations were performed at room temperature in 50 mM phosphate (pH 7.4) on samples that either had been deoxygenated by bubbling the suspensions with Ar for 60 min or were fully oxygenated by bubbling with O_2. Results were compared to calibration curves constructed using standard MDA solutions to obtain the apparent MDA concentrations in the experimental samples. These calibration curves were linear over the MDA concentration range of 1−60 μM.

Mathematical Analyses. Analyses of reaction kinetics were carried out by numerical integration of differential equations. Numerical calculations were carried out on a personal computer using MatLab 5.2.

RESULTS

Lipid Oxidation. Examination of Sephadex G-100 eluant fractions of PC that had been exposed to ONOOH revealed the presence of a soluble component with optical bands absorbing maximally at ~233 nm. The amount of absorbing material that was obtained increased with exposure to increasing amounts of ONOOH. These observations suggest that oxidation of the membrane phospholipid had occurred with formation of soluble fragments containing conjugated dienes (*41*). To assess the extent of oxidative damage, we determined the amounts of TBARS formed under various reaction conditions; because the analyses were based upon

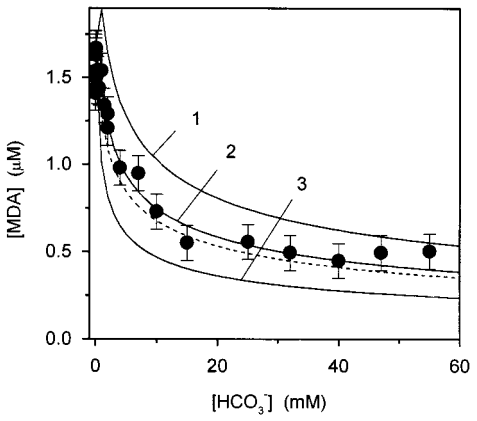

FIGURE 2: Bicarbonate dependence of the apparent MDA yield obtained upon addition of 1 mM peroxynitrite to 5 mg/mL suspensions of PC vesicles. The points show the experimental data, and the lines give the results of calculations using eq 13 where $k_1 = 0$, $k_{10} = 1.4 \times 10^6$ M^{-1} s^{-1}, and $k_{11} = 2.9 \times 10^7$ M^{-1} s^{-1} (curve 1), $k_{11} = 2.1 \times 10^7$ M^{-1} s^{-1} (curve 2), and $k_{11} = 1.2 \times 10^7$ M^{-1} s^{-1} (curve 3). The dashed line corresponds to $k_1 = 2.0 \times 10^4$ M^{-1} s^{-1}, $k_{10} = 0$, and $k_{11} = 2.1 \times 10^7$ M^{-1} s^{-1}.

reactions of MDA standards, the results are reported as apparent MDA concentrations. In the absence of bicarbonate, the MDA yields were linearly dependent upon the PC concentration over the measured range of 1−5 mg/mL and upon the peroxynitrite concentration over the range of 0.2−1 mM. TBARS analyses also were carried out with DPPC and DMPC vesicles; as expected, no oxidation products were obtained from vesicles containing the pure phospholipids, but apparent MDA formation was observed for mixed vesicles containing small amounts of PAPC. The MDA yield for a 19:1 DPPC/PAPC mixture (i.e., 5 mol % PAPC) increased linearly with increasing effective concentrations of PAPC over the range of 0.05−0.25 mg/mL. At saturating O_2 concentrations, the extent of damage increased relative to that measured in anaerobic vesicle solutions, but the magnitude of the effect was small, comprising on average an ~20% greater MDA yield. On a molar basis, the highest MDA yield obtained in these experiments was only ~0.1% of the added peroxynitrite.

The MDA yield decreased progressively with addition of increasing amounts of bicarbonate, as illustrated in Figure 2. These concentrations encompass the range generally found in physiological fluids. The data were analyzed according to a dynamical model that included as elementary reaction steps both direct oxidation of the vesicles by ONOOH:

$$\mathrm{ONOOH} + \mathrm{vesicle} \xrightarrow{k_1} \mathrm{MDA} \qquad (1)$$

and all relevant known reactions of the secondary radicals derived from the decomposition of ONOOH and $ONOOCO_2^-$ (i.e., $OH^\bullet$, $CO_3^{\bullet-}$, and $NO_2^\bullet$):

$$\mathrm{ONOOH} \xrightarrow{k_2,\gamma_1} \mathrm{OH}^\bullet + \mathrm{NO_2}^\bullet$$

$$\mathrm{ONOOH} \xrightarrow{k_2,1-\gamma_1} \mathrm{H}^+ + \mathrm{NO_3}^- \qquad (2)$$

$$\mathrm{ONOO}^- + \mathrm{CO_2} \xrightarrow{k_3,\gamma_2} \mathrm{CO_3}^{\bullet-} + \mathrm{NO_2}^\bullet$$

$$\mathrm{ONOO}^- + \mathrm{CO_2} \xrightarrow{k_3,1-\gamma_2} \mathrm{CO_2} + \mathrm{NO_3}^- \qquad (3)$$

For these reactions, the radical yields are as follows: $\gamma_1 = 0.28$ (*22*) and $\gamma_2 = 0.35$ (*14*). The complete set of reactions included in the calculations and their corrresponding rate constants are listed in the Appendix; for simplicity, only those steps for the reaction intermediates that computational analyses have shown represent the predominant decay pathways are given here. Hydroxyl radical is efficiently scavenged by NO_2^-:

$$OH^\bullet + NO_2^- \xrightarrow{k_4} OH^- + NO_2^\bullet \quad (4)$$

and, at high bicarbonate concentrations, by HCO_3^-:

$$OH^\bullet + HCO_3^- \xrightarrow{k_5} H_2O + CO_3^{\bullet-} \quad (5)$$

Carbonate radical decays primarily by radical recombination with $NO_2^\bullet$:

$$NO_2^\bullet + CO_3^{\bullet-} \xrightarrow{k_6} NO_3^- + CO_2 \quad (6)$$

and nitrogen dioxide decays primarily in a reaction sequence involving dimerization and hydrolytic disproportionation:

$$NO_2^\bullet + NO_2^\bullet \xrightarrow{k_7} N_2O_4 \quad (7)$$

$$N_2O_4 \xrightarrow{k_8} NO_2^\bullet + NO_2^\bullet \quad (8)$$

$$N_2O_4 + H_2O \xrightarrow{k_9} NO_2^- + NO_3^- + 2H^+ \quad (9)$$

Each of these radicals and N_2O_4 can, in principle, also react with the vesicles, oxidizing lipidic components to generate TBARS:

$$NO_2^\bullet + \text{vesicle} \xrightarrow{k_{10}} \text{MDA} \quad (10)$$

$$CO_3^{\bullet-} + \text{vesicle} \xrightarrow{k_{11}} \text{MDA} \quad (11)$$

$$OH^\bullet + \text{vesicle} \xrightarrow{k_{12}} \text{MDA} \quad (12)$$

where, in reaction 10, no distinction is made between $NO_2^\bullet$ and N_2O_4 as the oxidant. The MDA yield is then given by the equation

$$[\text{MDA}] = \int_0^\infty (k_1[\text{ONOOH}] + k_{10}[NO_2^\bullet] + k_{11}[CO_3^{\bullet-}] + k_{12}[OH^\bullet])[\text{ves}]\, dt \quad (13)$$

The rate constant for the reaction of $CO_3^{\bullet-}$ with the vesicles (k_{11}) can be determined by using eq 13 to fit the bicarbonate dependence of the MDA yield (Figure 2). From the MDA yield in bicarbonate-free media, the overall first-order decay by the other pathways (i.e., the sum of the k_1, k_{10}, and k_{12}) is calculated, which can then be used to set upper limits for the individual rate constants. Mathematically, the analysis consisted of calculating the concentration versus time profiles for the species ONOOH, $NO_2^\bullet$, $CO_3^{\bullet-}$, and $OH^\bullet$ by numerical solution of the differential equations describing their formation and decay (Appendix), followed by numerical evaluation of the integral in eq 13 using test values for k_1, k_{10}, k_{11}, and k_{12} until optimal fits to the experimental data were found.

Table 1: MDA Yield Obtained upon Oxidation of Vesicles by Peroxynitrite and Associated Rate Constants for ONOOH (k_1), $NO_2^\bullet$ (k_{10}), and $CO_3^{\bullet-}$ (k_{11})

membrane	oxidation yield[a]	k_1 ($\times 10^{-3}$ M^{-1} s^{-1})[b]	k_{10} (M^{-1} s^{-1})[b]	k_{11} ($\times 10^{-6}$ M^{-1} s^{-1})
egg PC	1.6×10^{-3}	23	24	23
DPPC/PAPC (19:1)	1.2×10^{-3}	8.2	6.5	7.0
DMPC/PAPC (19:1)	3.1×10^{-4}	2.6	2.5	2.1

[a] Reaction between 1 mM ONOOH and 3 mg/mL phospholipid in 50 mM phosphate at pH 7.4 and 21 °C. [b] Upper limits from Figure 3.

For these calculations, the initial concentrations of ONOOH, $ONOO^-$, and CO_2 were determined using a peroxynitrous acid dissociation constant K_a of 2.5×10^{-7} M (*42*) and the CO_2 hydration−dehydration equilibrium constant K of 1.1×10^{-6} M (*43*).

Data fits were very sensitive to the values chosen for k_{11}. Results shown in Figure 2 are representative; in this case, increasing k_{11} by ±50% caused a marked deviation of the calculated curve from the experimental values. In contrast, the value of k_{11} giving an acceptable fit was insensitive to the choice of bicarbonate-independent pathways included in the model. Thus, for example, nearly identical values for k_{11} were obtained when it was assumed that the bicarbonate-independent oxidative damage occurred exclusively by reaction of ONOOH (k_{10} and $k_{12} = 0$) or by reaction of $NO_2^\bullet$ (k_1 and $k_{12} = 0$) (Figure 2). Best-fit values for k_{11} determined by this analysis for egg PC liposomes and 19:1 DPPC/PAPC and 19:1 DMPC/PAPC vesicles are given in Table 1. In principle, $ONOOCO_2^-$ could also directly oxidize the vesicle lipids. However, the adduct lifetime is estimated to be on the order of 10^{-7} s (*16*), precluding significant amounts of it encountering a vesicle before decomposing. Specifically, the average diffusion distance calculated from its mean lifetime is ∼10 nm, whereas the distances between vesicles were typically 100−400 nm. These latter values are estimates based upon vesicle concentrations of 0.035−1.2 μM, calculated from the amount of added phospholipid (1.0−35 mg/mL), assuming an external vesicle diameter of 70 nm and a surfactant cross-sectional area of 0.69 nm^2 (*44*).

Scavenging of $OH^\bullet$ by NO_2^- to generate $NO_2^\bullet$ (reaction 4) and, at high bicarbonate concentrations, by HCO_3^- to generate $CO_3^{\bullet-}$ (reaction 5) is extensive under these conditions so that direct reaction with the vesicles by the k_{12} pathway should not contribute significantly to formation of TBARS. This expectation was confirmed in experiments where NO_2^- was added to carbonate-free reaction environments, thereby increasing the effectiveness of scavenging of $OH^\bullet$ without significantly altering the amounts of the other oxidants (ONOOH and $NO_2^\bullet$). Increasing the NO_2^- concentration to 1 mM, which ensured that virtually all the $OH^\bullet$ that formed would be scavenged, caused a decrease in the level of MDA of only ∼10% relative to the amount obtained in the absence of added nitrite. Thus, only a minor fraction of the MDA that formed could occur by direct reaction between $OH^\bullet$ and the vesicles. From these data, the value estimated for k_{12} was $\sim 10^{10}$ M^{-1} s^{-1}. The diffusion-controlled limit for reaction with the vesicles (k_D), calculated from the Einstein−Smoluchowski equation assuming a vesicle radius of 35 nm and a typical aqueous diffusion coefficient (*45*) for $OH^\bullet$ of 2×10^{-5} cm^2 s^{-1}, is $\approx 5 \times 10^{11}$ M^{-1} s^{-1}. Apparent

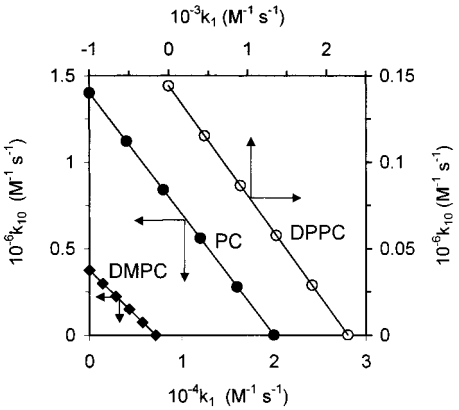

FIGURE 3: Correspondence between k_1 and k_{10} implied by the kinetic model for membrane oxidation: (◆) 19:1 DMPC/PAPC vesicles, (●) PC vesicles, and (○) 19:1 DPPC/PAPC vesicles.

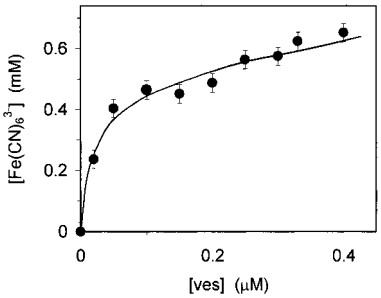

FIGURE 4: Dependence of $Fe(CN)_6^{3-}$ yield upon PC vesicle concentration. Vesicles at the indicated concentrations containing 0.2 M entrapped $Fe(CN)_6^{4-}$ reacted at 21 °C in 50 mM phosphate (pH 7.4) with 650 μM peroxynitrite. The line is the dependence calculated from the kinetic model.

MDA formation from reaction with $OH^{\bullet}$ is therefore relatively effective, requiring on average $\sim 10^2$ encounters per vesicle to generate a TBARS.

Our data do not allow discrimination between ONOOH and $NO_2^{\bullet}$ as lipid oxidants; however, useful boundaries for their reaction rate constants with vesicles can be set from the overall measured yields. By assuming that reaction occurs exclusively by only one oxidant or the other, upper limits for k_1 and k_{10} were calculated for each of the vesicles; the results are listed in Table 1. Relationships between the actual values for k_1 and k_{10} are also fixed by the total yield; these relationships for the three vesicle systems studies are displayed in Figure 3.

Transmembrane Oxidation of $Fe(CN)_6^{4-}$ by ONOOH. Addition of peroxynitrite to suspensions of phosphatidylcholine vesicles containing occluded $Fe(CN)_6^{4-}$ caused oxidation to $Fe(CN)_6^{3-}$ with yields [defined as the amount of $Fe(CN)_6^{3-}$ formed per the amount of ONOOH added] that were practically the same as that observed in a homogeneous solution. The yields were insensitive to the medium acidity over the pH range of 5−9, but increased with increasing concentrations of PC vesicles over the range of 0.035−1.2 μM in a manner predicted by the kinetic model described below (Figure 4). Stopped-flow kinetic analyses indicated that oxidation of entrapped $Fe(CN)_6^{4-}$ at pH 7.4 was first-order and occurred at the same rate as peroxynitrite decay. A representative trace is given in Figure 5. In separate experiments, it was determined that PC vesicles had no effect upon the kinetics of peroxynitrite decay, in both the presence

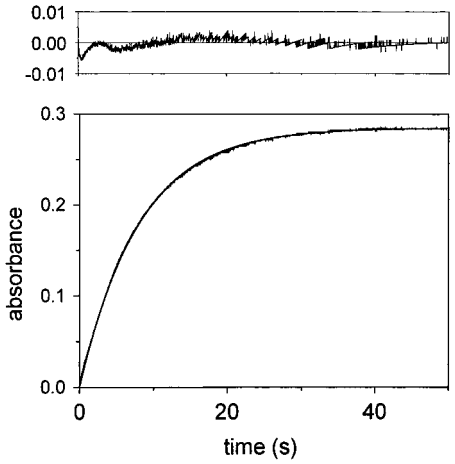

FIGURE 5: Kinetics of $Fe(CN)_6^{3-}$ formation by peroxynitrite in PC suspensions containing 0.2 M entrapped $Fe(CN)_6^{4-}$. The upper panel shows the residuals from the kinetic data fit assuming an exponential decay.

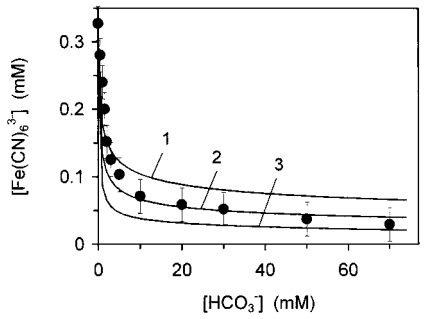

FIGURE 6: Bicarbonate dependence of the $Fe(CN)_6^{3-}$ yield obtained upon addition of 0.46 mM peroxynitrite to 5 mg/mL suspensions of PC vesicles containing 0.2 M entrapped $Fe(CN)_6^{4-}$. The points show the experimental data; the solid lines represent the results of calculations using eq 22 assuming that $k_d = 1 \times 10^6$ s^{-1} and $k_t = 2.5 \times 10^3$ s^{-1} (curve 1), $k_t = 5 \times 10^3$ s^{-1} (curve 2), and $k_t = 1 \times 10^4$ s^{-1} (curve 3).

and absence of bicarbonate. Similarly, the $Fe(CN)_6^{3-}$ yield obtained in a homogeneous solution was unaffected by addition of up to 1.2 μM (35 mg/mL) PC vesicles. These observations indicate that the lipid did not alter the oxidation yields by scavenging peroxynitrite. Following reaction with peroxynitrite, the $Fe(CN)_6^{4-}$-loaded PC vesicles were passed through Sephadex G-100 columns and the amount of entrapped $Fe(CN)_6^{3-}$ was determined spectrophotometrically. More than 90% of the oxidized product coeluted with the vesicles, indicating that they had remained intact, i.e., retained the complex ion, following treatment with peroxynitrite. Ferricyanide yields were typically ~10% lower when DPPC vesicles were used in place of egg PC.

Addition of physiologically relevant amounts of bicarbonate caused dramatic reductions in the yields of vesicle-entrapped $Fe(CN)_6^{3-}$, although the yields in a homogeneous solution were essentially unaffected. A typical result is given in Figure 6 for PC vesicles; a similar effect is observed for DPPC and DMPC vesicles. At pH 7.0, over the experimentally accessible bicarbonate range of 0−70 mM, the yields were reduced from 71 to 6.5% for PC, from 53 to 11% for DPPC, and from 65 to 9% for DMPC vesicles. Yields were unchanged within experimental uncertainty when the temperature was increased from 21 to 37 °C. As discussed below,

the extent of bicarbonate protection was used to determine the permeability coefficients for ONOOH across these membranes.

Transmembrane oxidation of $Fe(CN)_6^{4-}$ in the presence of bicarbonate was treated by assuming a conventional four-compartment model for diffusion across the bilayer (*46*, *47*), to which was added the known decay and appropriate redox reactions of ONOOH, $OH^{\bullet}$, $NO_2^{\bullet}$, and, when bicarbonate was present, the $ONOOCO_2^-$ adduct. In this model (Figure 1), ONOOH and $NO_2^{\bullet}$ located in the bulk external phase either diffuse to the aqueous−organic membrane interface:

$$ONOOH/NO_2^{\bullet}/N_2O_4 + \text{vesicle} \xrightarrow{k_{14}} ONOOH_{bo},\ NO_2^{\bullet}{}_{bo},\ N_2O_{4_{bo}} \quad (14)$$

or decay by the chemical transformations described above (reactions 1−9). The notation used in eq 14 and subsequent equations is that the subscripts bo and bi refer to reactants bound to the outer and inner membrane surfaces, respectively. The externally bound ONOOH and $NO_2^{\bullet}$ either dissociate from the vesicle:

$$ONOOH_{bo},\ NO_2^{\bullet}{}_{bo},\ N_2O_{4_{bo}} \xrightarrow{k_{15}} (ONOOH/NO_2^{\bullet}/N_2O_4) + \text{vesicle} \quad (15)$$

or diffuse across the bilayer to occupy an equivalent site on the inner vesicle surface:

$$ONOOH_{bo},\ NO_2^{\bullet}{}_{bo},\ N_2O_{4_{bo}} \xrightarrow{k_{16}} ONOOH_{bi},\ NO_2^{\bullet}{}_{bi},\ N_2O_{4_{bi}} \quad (16)$$

The internally bound ONOOH and/or $NO_2^{\bullet}$ can return to the outer vesicle surface:

$$ONOOH_{bi},\ NO_2^{\bullet}{}_{bi},\ N_2O_{4_{bi}} \xrightarrow{k_{17}} ONOOH_{bo},\ NO_2^{\bullet}{}_{bo},\ N_2O_{4_{bo}} \quad (17)$$

or react with $Fe(CN)_6^{4-}$ either directly:

$$ONOOH_{bi} + Fe(CN)_6^{4-} \xrightarrow{k_{18}} Fe(CN)_6^{3-} + NO_2^{\bullet}{}_{bi} + OH^- \quad (18)$$

$$NO_2^{\bullet}{}_{bi} + Fe(CN)_6^{4-} \xrightarrow{k_{19}} Fe(CN)_6^{3-} + NO_2^- \quad (19)$$

or indirectly via peroxynitrite decomposition to form $OH^{\bullet}{}_{bi}$, $NO_2^{\bullet}{}_{bi}$, and, when bicarbonate is present, $CO_3^{\bullet-}{}_{bi}$:

$$OH^{\bullet}{}_{bi} + Fe(CN)_6^{4-} \xrightarrow{k_{20}} Fe(CN)_6^{3-} + OH^- \quad (20)$$

$$CO_3^{\bullet-}{}_{bi} + Fe(CN)_6^{4-} \xrightarrow{k_{21}} Fe(CN)_6^{3-} + CO_3^{2-} \quad (21)$$

The internally bound ONOOH and radicals can also reversibly dissociate from the membrane surface and undergo all of the above chemical reactions within the inner aqueous phase of the vesicles. Transmembrane diffusion of $CO_3^{\bullet-}$ was not included in the kinetic scheme because, as a charged ion (*48*), its intrinsic diffusion rate is expected to be several orders of magnitude lower than those of the neutral species, ONOOH and $NO_2^{\bullet}$ (*49*).

Although the number of elementary reaction steps is quite large, it can be reduced to manageable proportions by introducing several reasonable simplifying assumptions. First, if it is assumed that the rate constants for reactions occurring within the inner aqueous phase are the same as those measured in bulk solution, all internal reactions of $OH^{\bullet}$, $NO_2^{\bullet}$, and $CO_3^{\bullet-}$ other than oxidation of $Fe(CN)_6^{4-}$ are insignificant and can be neglected. Second, $OH^{\bullet}$ generated in the external medium is too short-lived to diffuse across the membrane, and consequently, externally generated $OH^{\bullet}$ decays in the bulk volume. This assumption was confirmed by including in the calculations a pathway for transmembrane diffusion of $OH^{\bullet}$. Even when an unrealistically large diffusion coefficient (i.e., that of bulk water) was assumed, the same parameters giving the optimal data fit were obtained as when this pathway was omitted, indicating that transmembrane oxidation of $Fe(CN)_6^{4-}$ by externally generated $OH^{\bullet}$ could be ignored. Third, loss of ONOOH and $NO_2^{\bullet}$ by oxidation of membrane lipids was negligible because these processes are very inefficient. This assumption is consistent with the very low TBARS yields that were measured following exposure of the vesicles to peroxynitrite. Fourth, rates of decomposition and redox reactions involving the bound species are the same as those of the corresponding reactions in homogeneous solution. Given this set of assumptions, the rate constants for all of the chemical reactions can be assigned.

The extent of oxidation of $Fe(CN)_6^{4-}$ predicted by this simplified model is given by the following equation:

$$\frac{[Fe(CN)_6^{3-}]}{[Fe(CN)_6^{4-}]} = \int_0^{\infty} (k_{18}[ONOOH]_i + k_{19}[NO_2^{\bullet}]_i + k_{20}[OH^{\bullet}]_i + k_{21}[CO_3^{\bullet-}]_i)\, dt \quad (22)$$

where the subscript i now refers to the total internal concentration (i.e., membrane-bound plus dissociated) of the indicated species. Equation 22 was used to fit the dependence of the $Fe(CN)_6^{3-}$ yield on the bicarbonate concentration. As before, the fitting procedure consisted of calculating the time profiles for the concentrations of ONOOH and the radicals in all four compartments by numerical solution of the differential equations (listed in the Appendix) corresponding to all the processes in the system, followed by numerical integration of eq 22 until acceptable fits to the experimental data were obtained. For these calculations, the rate constants for diffusion from the inner aqueous phase to the inner surface (k_i) were estimated to be $6D/r_i^2$ ($=1.2 \times 10^7\ s^{-1}$; *50*), where the internal vesicle radius (r_i) was taken to be 31 nm (*44*). If it is assumed that the membrane asymmetry does not influence the reaction dynamics, i.e., that transmembrane diffusion of ONOOH and $NO_2^{\bullet}$ is the same in both directions and that the rate constants for dissociation of these species from the internal and external membrane surfaces are identical, the analysis requires assignment of only two interdependent adjustable parameters. These are the transmembrane diffusion constant (k_t) and the rate constant for

Table 2: Membrane Dissociation and Permeation Constants for ONOOH and $NO_2^{\bullet}$ [a]

membrane	log k_t (s^{-1})	log k_d (s^{-1})	log P ($cm\ s^{-1}$) [b]
egg PC	3.5 ± 1.3	6.0 ± 0.8	-2.9 ± 1.3
DPPC	3.0 ± 1.3	6.0 ± 0.8	-3.4 ± 1.3
DMPC	3.2 ± 1.3	6.0 ± 0.8	-3.2 ± 1.3

[a] Reaction between 0.5 mM peroxynitrite and 5 mg/mL phospholipid in 50 mM phosphate at pH 7.4 and 21 °C. [b] Permeability coefficient (P), defined as $P = dk_t$ where d (=4 nm) is the bilayer width (*44*).

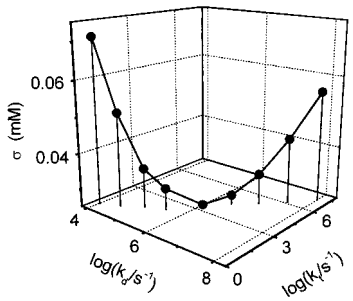

FIGURE 7: Deviations between experimental and calculated $Fe(CN)_6^{4-}$ oxidation yields for different values of membrane dissocation rate constants (k_d) for $NO_2^{\bullet}$ and ONOOH and the corresponding optimal values of their transmembrane rate constants (k_t).

dissociation from the vesicle surface (k_d). Note that this analysis cannot distinguish among ONOOH, $NO_2^{\bullet}$, and N_2O_4 as the actual diffusing species. The calculated rate constants are therefore apparent values that represent the cumulative diffusion of all of the neutral oxidants.

Best-fit values obtained from the analyses for egg PC, DMPC, and DPPC vesicles are listed in Table 2. A comparison with the experimental data for transmembrane oxidation of $Fe(CN)_6^{4-}$ in PC liposomes is given in Figure 6 (curve 2); also shown are calculated curves for suboptimal values of k_t (curves 1 and 3). One surprising result of these calculations is that the same optimal values of k_t and k_d were obtained when it was assumed that reaction with $Fe(CN)_6^{4-}$ occurred only at the internal membrane surface; i.e., the result was not dependent upon the internal location of the oxidant.

To assess the accuracy of the results, we calculated the sum of deviations (σ) between the calculated and experimental values of the $Fe(CN)_6^{3-}$ concentration that gave optimal values for k_t at various fixed values of k_d:

$$\sigma^2 = (1/n)\sum_{i=1}^{n}([Fe(CN)_6^{3-}]_i^{exp} - [Fe(CN)_6^{3-}]_i^{calc})^2$$

thereby obtaining the dependence of σ on the chosen values of k_t and k_d. The results are displayed in Figure 7, from which it is possible to estimate error limits for k_t and k_d. The standard deviations (σ) for individual data points obtained for each HCO_3^- concentration are 0.03 mM; the limits cited in Table 2 represent the corresponding uncertainty in k_t and k_d.

The mechanism (Figure 1) also predicts that addition of a sufficient amount of NO_2^- to effectively scavenge $CO_3^{\bullet -}$, i.e., the reaction

$$CO_3^{\bullet -} + NO_2^- \xrightarrow{k_{23}} CO_3^{2-} + NO_2^{\bullet} \qquad (23)$$

will reverse the protective effect observed in bicarbonate-containing solutions. Thus, in solutions containing both CO_2 and NO_2^-, peroxynitrite will be converted primarily to $NO_2^{\bullet}$ which, if membrane-permeable, will undergo transmembrane diffusion in competition with hydrolytic disproportionation (reactions 7 and 9) to oxidize occluded $Fe(CN)_6^{4-}$. As illustrated in Figure 8, this effect is observed and can be quantitatively modeled using the constants k_t and k_{-d} determined from the bicarbonate inhibition studies (Table 2).

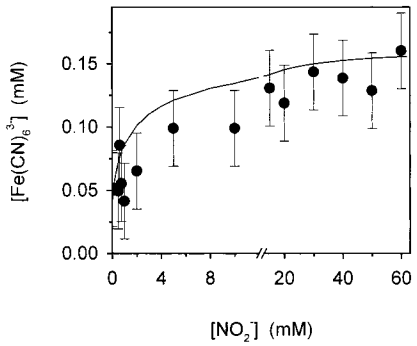

FIGURE 8: Nitrite dependence of the $Fe(CN)_6^{3-}$ yield obtained upon addition of 0.46 mM peroxynitrite to 5 mg/mL suspensions of PC vesicles containing 0.2 M entrapped $Fe(CN)_6^{4-}$ in 50 mM phosphate/30 mM bicarbonate buffer (pH 7.4). The points show the experimental data; the solid lines give the results of calculations using eq 22 assuming that $k_d = 1 \times 10^6\ s^{-1}$ and $k_t = 5 \times 10^3\ s^{-1}$.

DISCUSSION

Transmembrane Diffusion of Peroxynitrite. The most striking result from these studies is that transmembrane oxidation by peroxynitrite was extremely facile, with the membrane presenting no significant barrier to reaction with vesicle-entrapped $Fe(CN)_6^{4-}$ in the absence of bicarbonate. Our data confirm earlier observations by Groves and coworkers (*32*), who made use of large liposomes prepared in a different manner and an entirely different chemical trapping system. It is not possible with the data from either study to determine quantitatively the relative contributions of ONOOH or $NO_2^{\bullet}$ to transmembrane oxidation. However, there is a priori no reason to exclude participation by either of them, since both should be membrane-permeable and $NO_2^{\bullet}$ is sufficiently long-lived to traverse the bilayer. Indeed, we were able to obtain acceptable fits to the dependence of the $Fe(CN)_6^{3-}$ yield on bicarbonate concentration (Figure 6) only when contributions from both ONOOH and externally generated $NO_2^{\bullet}$ to the oxidation of internal $Fe(CN)_6^{4-}$ were included in our calculations (data not shown). The ability of $NO_2^{\bullet}$ to permeate the bilayer was clearly demonstrated by reversal of bicarbonate-dependent product inhibition upon addition of excess NO_2^- (Figure 8). Under these experimental conditions, virtually all of the extracellular ONOOH was converted via the intermediacy of $ONOOCO_2^-$ to $NO_2^{\bullet}$ before transmembrane diffusion could occur (Figure 1).

Our observation that adding physiological quantities of bicarbonate to the medium markedly protected the vesicle-entrapped $Fe(CN)_6^{4-}$ differs from those of Groves and coworkers (*32*), who reported that added bicarbonate had no effect on transmembrane oxidation in their system. One possible explanation for the differences is effective scavenging of $CO_3^{\bullet -}$ in their system by reaction 23, although they

do not report the level of NO_2^- contamination in their ONOOH preparations. In our study, protection was not a consequence of limiting access of peroxynitrite to the vesicles by shortening its lifetime. Under the most restrictive conditions of our study, CO_2-catalyzed isomerization of $ONOO^-$ to NO_3^- reduces the peroxynitrite lifetime to 3−6 ms, corresponding to an average diffusion distance in homogeneous solution of ~7 μm. At the lowest PC concentrations used in these studies (1 mg/mL), there are $\sim 2 \times 10^{13}$ vesicles/mL, whose average separation distance is calculated to be <0.5 μm. Thus, the added peroxynitrite has access to the vesicles in suspension under all experimental conditions. Protection by bicarbonate is observed because diffusion across the bilayer occurs on the same time scale as CO_2-catalyzed isomerization. Thus, using our kinetic model (Figure 1), it is possible to estimate from the magnitude of inhibition of $Fe(CN)_6^{3-}$ formation the effective transmembrane diffusion coefficients of ONOOH and $NO_2^\bullet$. These values, listed in Table 2, are very similar to the value reported by Groves and co-workers (*32*) and are 1−2 orders of magnitude larger than those usually measured for polar nonelectrolytes moving through planar lipid bilayers (*34*). The data provide two independent checks on the self-consistency of the rate parameters calculated from the model. First, with these values the model accurately reproduces the observed dependence of the $Fe(CN)_6^{3-}$ yield on PC vesicle concentration (Figure 4). Second, from the MDA yield obtained with $OH^\bullet$, one estimates that $k_d/k_t \approx 10^2$, which is the ratio calculated from the transmembrane oxidation results (Table 2). In our study, the permeabilities increased with decreasing membrane microviscosity, which follows the order DPPC > DMPC > PC, although the effect is small, presumably because the energetic barrier to diffusion is not large. The large k_t values are consistent with the notion that diffusion of $NO_2^\bullet$ is a major pathway for transmembrane oxidation and reduction since it is well-established that other small molecules exhibit anomalously high membrane permeabilities (*34*).

A result that has puzzled the scientific community is that transmembrane diffusion of the oxidant is insensitive to pH, at least as measured by the product yields of entrapped reductants. In our study, the $Fe(CN)_6^{4-}$ yield was essentially unchanged when the medium acidity was varied over the pH range of 5−9. Since the pK_a for peroxynitrous acid is 6.6 (*42*), this means that the yield was insensitive to the extent of protonation of peroxynitrite, which changed from 98% ONOOH to 99% $ONOO^-$ over the full pH range. Our kinetic results (Figure 5) establish that diffusion is electroneutral, i.e., involves uncharged species. Any significant diffusion of $ONOO^-$ that was not accompanied by charge-compensating diffusion of the electrolyte would lead to development of a transmembrane potential opposing further $ONOO^-$ diffusion. This effect, when present, is apparent in kinetic profiles for transmembrane oxidation and reduction, which show marked departures from first-order behavior (*51*). Since the curves are strictly first-order for transmembrane transfer of up to 1.5×10^3 electrons per vesicle, it is clear that the reaction does not involve net translocation of charge. Beckman and co-workers (*33*) have suggested that $ONOO^-$ forms an ion pair with electrolyte cations, e.g., Na^+, which is membrane-permeable. This strikes us as inherently unreasonable, given the very low ligand binding affinities of alkali metal ions and their high hydrophilicities. Groves and co-workers (*32*) have suggested that the apparent pK_a for ONOOH might be shifted to higher values at the membrane interface so that the interfacial oxidant is largely protonated in weakly alkaline solutions. In this case, a shift of two units in pK_a to ~8.8, which is the minimum necessary to account for the data, would require an interfacial potential of −120 mV, which is exceptionally large for a formally uncharged membrane interface (*52*). Furthermore, incorporation of stearylamine did not alter their results, although a positively charged membrane would decrease the apparent pK_a of bound peroxynitrite by excluding protons from the interfacial region. A simple alternative explanation relies upon recognition that the product yield is a ratio of the rate of transmembrane oxidation and reduction to the overall rate of decomposition by all available pathways. The rates of peroxynitrite isomerization to NO_3^- and oxidation of $Fe(CN)_6^{4-}$ are both dependent on the fraction present as ONOOH. Consequently, no pH dependence is observed on the $Fe(CN)_6^{3-}$ yield in homogeneous solution. Under our experimental conditions, $k_t \sim 10^3\ s^{-1}$ (Table 2) and the apparent first-order rate constant for $Fe(CN)_6^{4-}$ oxidation by ONOOH, given by $k_{18}[Fe(CN)_6^{4-}]$, is $\sim 2\ s^{-1}$ ($\ll k_t$) when the internal $Fe(CN)_6^{4-}$ concentration is 0.2 M. On average, then, the oxidant could cross the membrane as many as several hundred times before reacting. Under these circumstances, the reaction by this pathway would behave dynamically as if the membrane were absent. In contrast, $k_{19}[Fe(CN)_6^{4-}] \sim 4 \times 10^5\ s^{-1}$ ($\gg k_t$) under these conditions so that $NO_2^\bullet$ is efficiently scavenged by $Fe(CN)_6^{4-}$, reacting virtually every time it crosses the membrane. Rate-limiting transmembrane diffusion of $NO_2^\bullet$ is not expected to be pH-dependent. However, its rate of formation by ONOOH decomposition, and hence its flux across the bilayer, decreases with increasing pH. Consequently, the relative rates of $Fe(CN)_6^{4-}$ reduction by ONOOH and $NO_2^\bullet$ and, correspondingly, the $Fe(CN)_6^{4-}$ yields are not expected to be very pH-sensitive.

Membrane Damage. Peroxynitrite-induced oxidation of membrane lipids in erythrocytes (*53*), mitochondria (*54*), and soybean PC (*55*) has been reported. In cells and biological membranes, this is accompanied by damage to integral membrane proteins (e.g., the preceding references and refs *56*−*58*). In artificial liposomes, oxidizable lipid-soluble biomolecules can be protected from peroxynitrite degradation by addition of interfacially bound metalloporphyrins (*59*), and bicarbonate has been shown to inhibit oxidation of oxyhemoglobin to its met form in erythrocytes (*8*). In this study, we find that bicarbonate also protects the membrane polyalkenyl chains from oxidative damage. In the erythrocyte system (*8*), protection could be attributed in part to diffusion limitations, i.e., CO_2-catalyzed isomerization of peroxynitrite to nitrate before it could reach its biological target sites. This complicating feature was not present in our study in which we used small vesicles whose average separation distance was correspondingly much shorter. Consequently, we were able to estimate the reactivity of peroxynitrite toward the membrane lipids in terms of a simple scheme involving concurrent reactions of the vesicles directly with ONOOH and with radicals derived from its decomposition. The linear

increase in MDA yield with increasing amounts of added peroxynitrite at fixed PC concentrations indicates that the extent of oxidative damage was not saturating under these conditions. The linear increase in MDA yield with increasing PC concentration at a fixed peroxynitrite concentration indicates that the reaction is first-order in PC. Free radical chain reactions involving O_2 apparently make only minor contributions to the overall oxidative damage, since the yields were only slightly higher in O_2-saturated media than in anaerobic media. From the bicarbonate and nitrite concentration dependences of the oxidation yields, apparent rate constants for MDA formation by reaction with $OH^•$ and $CO_3^{•-}$ were determined; unique values for the constants for reaction with ONOOH and $NO_2^•$ were not obtained, but upper limits could be set from relationships inherent in the kinetic model. The rate constants for membrane oxidation varied according to the intrinsic reactivities of the various oxidants toward organic molecules, i.e., $OH^• > CO_3^{•-} >$ ONOOH and $NO_2^•$. Nonetheless, the extent of damage to the vesicles varied in the inverse order; i.e., $OH^•$ caused very little damage, and $CO_3^{•-}$ formation partially protected against ONOOH (Figure 2). This somewhat counterintuitive result arises because the more reactive oxidants are also more effectively scavenged by various medium components than are the less reactive ones. Ultimately, this leads to accumulation of the relatively stable oxidant, $NO_2^•$, which then reacts with the vesicles.

Concluding Comments. We have developed a kinetic model based upon current conceptual viewpoints of membrane dynamics and peroxynitrite reaction mechanisms that accurately describes both lipid oxidation and transmembrane oxidations in vesicular assemblies, including the dramatic modulating effects of CO_2 and NO_3^- upon product yields. According to this model, the neutral species ONOOH and $NO_2^•$ rapidly permeate the bilayer, but the anionic species $ONOO^-$ and $CO_3^{•-}$ are membrane-impermeable. Protection of both membrane lipids and internal reductants arising from competitive CO_2-catalyzed isomerization to NO_3^- is extensive at physiologically relevant bicarbonate levels. Nonetheless, a significant fraction of the oxidant survives to cross the bilayer or attack vulnerable lipidic components. Successful application of the model to this complex reaction milieu also constitutes support for the general viewpoint presented in the introductory section that the so-called "indirect" reactions of peroxynitrite proceed via homolysis of the O−O peroxo bonds of ONOOH and $ONOOCO_2^-$. Refinement of the kinetic model for transmembrane diffusion of peroxynitrite will require independent study of the membrane diffusional behavior of $NO_2^•$. Finally, quantitative models of oxidative damage that restrict reactivity to confined spaces such as phagosomes (*60*) or interstitial fluids will need to be modified to take into account membrane permeation by peroxynitrite.

APPENDIX

The kinetic equations described below incorporate the following reaction steps not listed in the body of the text:

$$OH^• + OH^• \xrightarrow{k_{24}} H_2O_2 \quad (24)$$

$$OH^• + CO_3^{•-} \xrightarrow{k_{25}} \text{products} \quad (25)$$

$$CO_3^{•-} + CO_3^{•-} \xrightarrow{k_{26}} \text{products} \quad (26)$$

Calculations showed that, under the experimental conditions, these steps made only very minor contributions to the overall reaction, but they are included here to provide a general set of equations that describe the reaction dynamics of these processes.

Oxidation of Membrane Lipids. The following set of differential equations describes the changes in reactant concentrations associated with TBARS formation:

$$\frac{d[PN]}{dt} = -(k'_2 + k'_3[HCO_3^-] + k'_1[ves])[PN] \quad (A1.1)$$

$$\frac{d[OH^•]}{dt} = k'_2\gamma_1[PN] - (k_4[NO_2^-] + k_5[HCO_3^-] + k_{12}[ves] + k_{24}[OH^•] + k_{25}[CO_3^{•-}])[OH^•] \quad (A1.2)$$

$$\frac{d[NO_2^•]}{dt} = k'_2\gamma_1[PN] + k'_3\gamma_2[PN][HCO_3^-] + k_4[OH^•][NO_2^-] + 2k_8[N_2O_4] + k_{23}[CO_3^{•-}][NO_2^-] - (k_7[NO_2^•] + k_4[CO_3^{•-}] + k_{10}[ves])[NO_2^•] \quad (A1.3)$$

$$\frac{d[CO_3^{•-}]}{dt} = k'_3\gamma_2[PN] + k_5[OH^•][HCO_3^-] - (k_6[NO_2^•] - k_{23}[NO_2^-] - k_{25}[OH^•] - k_{26}[CO_3^{•-}] - k_{11}[ves])[CO_3^{•-}] \quad (A1.4)$$

$$\frac{d[NO_2^-]}{dt} = k_9[N_2O_4] - (k_4[OH^•] + k_{23}[CO_3^{•-}])[NO_2^-] \quad (A1.5)$$

$$\frac{d[N_2O_4]}{dt} = k_7[NO_2^•]^2 - (k_8 + k_9)[N_2O_4] \quad (A1.6)$$

In these equations, [PN] (=[ONOOH] + $[ONOO^-]$) is the total amount of the peroxynitrite, $[HCO_3^-]$ is the amount of added bicarbonate, [ves] is the vesicle concentration, $k'_1 = k_1/(1 + K_a/[H^+])$, $k'_2 = k_2/(1 + K_a/[H^+])$, and $k'_3 = k_3/(1 + [H^+]/K_a)/(1 + K/[H^+])$. Initially, $[PN]_{t=0} = [PN]_0$ and $[NO_2^-]_{t=0} = [NO_2^-]_0$, with the concentrations of all other reacting species being equal to zero. The rate constants used for the calculations are as follows: $k_1 = k_D = 5 \times 10^{11}$ M^{-1} s^{-1} and $k_2 = 0.9$ s^{-1} (*42*), $k_3 = 2.9 \times 10^4$ M^{-1} s^{-1} (*9*), $k_4 = 7.3 \times 10^9$ M^{-1} s^{-1} (*22*), $k_5 = 8.5 \times 10^6$ M^{-1} s^{-1} (*48*), $k_6 = 1.0 \times 10^9$ M^{-1} s^{-1} (*61*), $k_7 = 4.5 \times 10^8$ M^{-1} s^{-1} (*62*, *63*), $k_8 = 6.9 \times 10^3$ s^{-1} (*62*), $k_9 = 1.0 \times 10^3$ s^{-1} (*62*), $k_{23} = 6.6 \times 10^5$ M^{-1} s^{-1} (*64*), $k_{24} = 4.2 \times 10^9$ M^{-1} s^{-1} (*65*), $k_{25} = 3 \times 10^9$ M^{-1} s^{-1} (*66*), and $k_{26} = 2 \times 10^7$ M^{-1} s^{-1} (*67*). The yields of reactions 2 and 3 (γ_1 and γ_2) are 0.28 (*22*) and 0.35 (*14*), respectively.

Intravesicular Oxidation of $Fe(CN)_6^{4-}$. The set of differential equations used to describe changes in reactant concentrations in the vesicular system is given below. As noted in the text, the same transmembrane diffusion rate for the oxidant was obtained when it was assumed that all reactions within the vesicle occurred from the inner surface as when the full kinetic treatment that included separate reactions in the inner aqueous core and on the inner membrane surface was used. Consequently, only the mathematically less cumbersome equations corresponding to the simplified model are shown here.

Reactions in the bulk aqueous phase:

$$\frac{d[PN]}{dt} = -(k'_2 + k'_3[HCO_3^-] + k'_{14}[ves])[PN] + k'_{15a}[PN]_{bo} \quad (A2.1)$$

$$\frac{d[OH^\bullet]}{dt} = k'_2\gamma_1[PN] - (k_4[NO_2^-] + k_{24}[OH^\bullet] + k_{25}[CO_3^{\bullet-}])[OH^\bullet] \quad (A2.2)$$

$$\frac{d[NO_2^\bullet]}{dt} = k'_2\gamma_1[PN] + k'_3\gamma_2[PN][HCO_3^-] + 2k_8[N_2O_4] + k_4[OH^\bullet][NO_2^-] + k_{23}[CO_3^{\bullet-}][NO_2^-] + k_{15b}[NO_2^\bullet]_{bo} - (k_6[CO_3^{\bullet-}] + k_7[NO_2^\bullet] + k_{14}[ves])[NO_2^\bullet] \quad (A2.3)$$

$$\frac{d[CO_3^{\bullet-}]}{dt} = k'_3\gamma_2[PN] + k_5[OH^\bullet][HCO_3^-] - (k_6[NO_2^\bullet] + k_{23}[NO_2^-] + k_{25}[OH^\bullet] + k_{26}[CO_3^{\bullet-}])[CO_3^{\bullet-}] \quad (A2.4)$$

$$\frac{d[NO_2^-]}{dt} = k_9[N_2O_4] - (k_4[OH^\bullet] + k_{23}[CO_3^{\bullet-}])[NO_2^-] \quad (A2.5)$$

$$\frac{d[N_2O_4]}{dt} = k_7[NO_2^\bullet]^2 + k_{15c}[N_2O_4]_{bo} - (k_8 + k_9 + k_{14}[ves])[N_2O_4] \quad (A2.6)$$

Reactions on the external membrane surface:

$$\frac{d[PN]_{bo}}{dt} = k'_{14}[ves][PN] + k'_{17a}[PN]_{bi} - (k_{15a} + k_{16a})[PN]_{bo} \quad (A2.7)$$

$$\frac{d[NO_2^\bullet]_{bo}}{dt} = k_{14}[ves][NO_2^\bullet] + k_{17b}[NO_2^\bullet]_{bi} - (k_{15b} + k_{16b})[NO_2^\bullet]_{bo} \quad (A2.8)$$

$$\frac{d[N_2O_4]_{bo}}{dt} = k_{14}[ves][N_2O_4] + k_{17c}[N_2O_4]_{bi} - (k_{15c} + k_{16c})[N_2O_4]_{bo} \quad (A2.9)$$

Reactions on the inner membrane surface:

$$\frac{d[PN]_{bi}}{dt} = k_{16a}[PN]_{bo} - (k'_{17a} + k'_2 + k'_3[HCO_3^-] + k'_{18}[Fe(CN)_6^{4-}])[PN]_{bi} \quad (A2.10)$$

$$\frac{d[OH^\bullet]_{bi}}{dt} = k'_2\gamma_1[PN]_{bi} - k_{20}[Fe(CN)_6^{4-}][OH^\bullet]_{bi} \quad (A2.11)$$

$$\frac{d[NO_2^\bullet]_{bi}}{dt} = k'_2\gamma_1[PN]_{bi} + k'_3\gamma_2[PN]_{bi}[HCO_3^-] + 2k_8[N_2O_4]_{bi} + k_{16c}[NO_2^\bullet]_{bo} - (k_{17c} + k_{19}[Fe(CN)_6^{4-}])[NO_2^\bullet]_{bi} \quad (A2.12)$$

$$\frac{d[CO_3^{\bullet-}]_{bi}}{dt} = k'_3\gamma_2[PN]_{bi} - k_{21}[Fe(CN)_6^{4-}][CO_3^{\bullet-}] \quad (A2.13)$$

$$\frac{d[N_2O_4]_{bi}}{dt} = k_{17c}[N_2O_4]_{bo} - k_{16c}[N_2O_4]_{bi} \quad (A2.14)$$

$$\frac{d[Fe(CN)_6^{3-}]}{dt} = (2k_{18}[PN]_{bi} + k_{19}[NO_2^\bullet]_{bi} + k_{20}[OH^\bullet]_{bi} + k_{21}[CO_3^{\bullet-}]_{bi})[Fe(CN)_6^{4-}] \quad (A2.15)$$

In this model, the rate constants for association at the membrane surface (k_{14}) are assumed to be equal for all of the membrane-permeable species and to be diffusion-limited, for which k_{14} ($=k_D$) $\approx 7 \times 10^{11}$ M^{-1} s^{-1}. In addition to the constants enumerated in section A1, the following rate constants were used for the calculations: $k_{18} = 8.2$ M^{-1} s^{-1} (*22*), $k_{19} = 2.1 \times 10^6$ M^{-1} s^{-1} (*63*), $k_{20} = 1.1 \times 10^{10}$ M^{-1} s^{-1} (*68*), and $k_{21} = 3.6 \times 10^8$ M^{-1} s^{-1} (*64*).

As discussed in the text, the following simplifying assumptions were made to reduce the number of variables: (i) $k_{16a} = k_{17a}$, $k_{16b} = k_{17b}$, and $k_{16c} = k_{17c}$; (ii) $k_{16a} = k_{16b} = k_{16c}$; and (iii) $k_{15a} = k_{15b} = k_{15c}$. With these assumptions, k_{16a}–k_{17c} can be replaced with an apparent transmembrane diffusion constant (k_t) and k_{15a}–k_{15c} with an "average" dissociation constant (k_d). In these equations, $k'_{14} = k_{14}/(1 + K_a/[H^+])$, $k'_d = k_d/(1 + K_a/[H^+])$, $k'_t = k_t/(1 + K_a/[H^+])$, and $k'_{18} = k_{18}/(1 + K_a/[H^+])$. The initial reaction conditions are as follows: $[PN]_{t=0} = [PN]_0$, $[NO_2^-]_{t=0} = [NO_2^-]_0$, $[HCO_3^-]_t = [HCO_3^-]_0$ is assumed to be constant, with the initial concentrations of other reactants set at zero. Note also that in this kinetic model it is assumed that N_2O_4 does not react directly with $Fe(CN)_6^{4-}$ (e.g., eq A2.14).

Validity of Steady-State Approximations. The steady-state approximation is often applied to the dynamical equations describing short-lived radicals to simplify the overall rate laws. This approximation is valid only if the rate of production of the reactive intermediate becomes equal to its rate of decay very early in the reaction. To examine whether steady-state conditions are achieved in these reactions, we have calculated temporal profiles for generation and decay of the short-lived radicals involved in these reactions. We have found that for $NO_2^\bullet$ and $CO_3^{\bullet-}$, the difference between the rates of formation and decay is significant at times shorter than 1 ms, which is comparable to their calculated lifetimes

($t_{1/2} \approx 10-20$ ms); thus, application of the steady-state approximation to reactions of these radicals is questionable. Only for $OH^{\bullet}$ is the steady-state approximation a valid assumption under the experimental conditions.

ACKNOWLEDGMENT

We are grateful to Jeremiah Halstead and Donna Wright for conducting preliminary experiments that established the feasibility of these studies.

REFERENCES

1. Beckman, J. S., and Koppenol, W. H. (1996) *Am. J. Physiol. 271*, C1424−C1437.
2. Ischiropoulos, H. (1998) *Arch. Biochem. Biophys. 356*, 1−11.
3. Hurst, J. K., and Lymar, S. V. (1999) *Acc. Chem. Res. 32*, 520−528.
4. Koppenol, W. H., Moreno, J. J., Pryor, W. A., Ischiropoulos, H., and Beckman, J. S. (1992) *Chem. Res. Toxicol. 5*, 834−842.
5. Huie, R. E., and Padmaja, S. (1993) *Free Radical Res. Commun. 18*, 195−199.
6. Lymar, S. V., and Hurst, J. K. (1996) *Chem. Res. Toxicol. 9*, 845−850.
7. Arteel, G. E., Briviba, K., and Sies, H. (1999) *FEBS Lett. 445*, 226−230.
8. Romero, N., Denicola, A., Souza, J. M., and Radi, R. (1999) *Arch. Biochem. Biophys. 368*, 23−30.
9. Lymar, S. V., and Hurst, J. K. (1995) *J. Am. Chem. Soc. 117*, 8867−8868.
10. Denicola, A., Freeman, B. A., Trujillo, M., and Radi, R. (1996) *Arch. Biochem. Biophys. 333*, 49−58.
11. Uppu, R. M., Squadrito, G. L., and Pryor, W. A. (1996) *Arch. Biochem. Biophys. 327*, 335−343.
12. Houk, K. N., Condroski, K. R., and Pryor, W. A. (1996) *J. Am. Chem. Soc. 118*, 13002−13006.
13. Goldstein, S., and Czapski, G. (1998) *J. Am. Chem. Soc. 120*, 3458−3463.
14. Lymar, S. V., and Hurst, J. K. (1998) *Inorg. Chem. 37*, 294−301.
15. Bonini, M. G., Radi, R., Ferrer-Sueta, G., Ferreira, A. M. D. C., and Augusto, O. (1999) *J. Biol. Chem. 274*, 10802−10806.
16. Merenyi, G., and Lind, J. (1997) *Chem. Res. Toxicol. 10*, 1216−1220.
17. Koppenol, W. H., and Kissner, R. (1998) *Chem. Res. Toxicol. 11*, 87−90.
18. Beckman, J. S., Beckman, T. W., Chen, J., Marshall, P. M., and Freeman, B. A. (1990) *Proc. Natl. Acad. Sci. U.S.A. 87*, 1620−1624.
19. Goldstein, S., and Czapski, G. (1999) *J. Am. Chem. Soc. 121*, 2444−2447.
20. Coddington, J. W., Lymar, S. V., and Hurst, J. K. (1999) *J. Am. Chem. Soc. 121*, 2438−2443.
21. Goldstein, S., Meyerstein, D., van Eldik, R., and Czapski, G. (1999) *J. Phys. Chem. A 103*, 6587−6590.
22. Gerasimov, O. V., and Lymar, S. V. (1999) *Inorg. Chem. 38*, 4317−4321.
23. Hodges, G. R., and Ingold, K. U. (1999) *J. Am. Chem. Soc. 121*, 10695−10710.
24. Zhu, L., Gunn, C., and Beckman, J. S. (1992) *Arch. Biochem. Biophys. 298*, 452−457.
25. Brunelli, L., Crow, J. P., and Beckman, J. S. (1995) *Arch. Biochem. Biophys. 316*, 327−334.
26. Hurst, J. K., and Lymar, S. V. (1997) *Chem. Res. Toxicol. 10*, 802−810.
27. Wolcott, R. G., Franks, B. S., Hannum, D. S., and Hurst, J. K. (1994) *J. Biol. Chem. 269*, 9721−9728.
28. Lymar, S. V., Jiang, Q., and Hurst, J. K. (1996) *Biochemistry 35*, 7855−7861.
29. Denicola, A., Rubbo, H., Rodriguez, D., and Radi, R. (1993) *Arch. Biochem. Biophys. 304*, 279−286.
30. Pryor, W. A., Lemercier, J.-N., Zhang, H., Uppu, R. M., and Squadrito, G. L. (1997) *Free Radical Biol. Med. 23*, 331−338.
31. Denicola, A., Souza, J. M., and Radi, R. (1998) *Proc. Natl. Acad. Sci. U.S.A. 95*, 3566−3571.
32. Marla, S. S., Lee, J., and Groves, J. T. (1997) *Proc. Natl. Acad. Sci. U.S.A. 94*, 14243−14248.
33. Macfadyen, A. J., Reiter, C., Zhuang, Y., and Beckman, J. S. (1999) *Chem. Res. Toxicol. 12*, 223−229.
34. Walter, A., and Gutknecht, J. (1986) *J. Membr. Biol. 90*, 207−217.
35. Singleton, W. S., Gray, M. S., Brown, M. L., and White, J. L. (1965) *J. Am. Oil Chem. Soc. 42*, 53−56.
36. Mayer, L. D., Hope, M. J., and Cullis, P. R. (1986) *Biochim. Biophys. Acta 858*, 161−168.
37. Saha, A., Goldstein, S., Cabelli, D., and Czapski, G. (1998) *Free Radical Biol. Med. 24*, 653−659.
38. Hughes, M. N., and Nicklin, H. G. (1968) *J. Chem. Soc. A*, 450−452.
39. Greenbert, A. E., Conners, J. J., and Jenkins, D. (1995) *Standard Methods for the Examination of Water and Wastewater*, 15th ed., pp 4-83, 4-84, 4-99, United Book Press, Baltimore.
40. Ohkawa, H., Ohishi, N., and Yagi, K. (1979) *Anal. Biochem. 95*, 351−358.
41. Klein, R. A. (1970) *Biochim. Biophys. Acta 210*, 486−489.
42. Edwards, J. O., and Plumb, R. C. (1994) *Prog. Inorg. Chem. 41*, 599−635.
43. Harned, H. C., and Bonner, F. C. (1945) *J. Am. Chem. Soc. 67*, 1026−1031.
44. Huang, C., and Mason, J. T. (1978) *Proc. Natl. Acad. Sci. U.S.A. 75*, 308−310.
45. Wilkinson, F. (1980) *Chemical Kinetics and Reaction Mechanisms*, p 140, Van Nostrand Reinhold, New York.
46. Byrne, J. H. (1988) *An Introduction to Membrane Transport and Bioelectricity*, Raven Press, New York.
47. Males, R. G., Phillips, P. S., and Herring, F. G. (1998) *Biophys. Chem. 70*, 65−74.
48. Czapski, G., Lymar, S. V., and Schwarz, H. A. (1999) *J. Phys. Chem. A 103*, 3447−3450.
49. Hurst, J. K., and Khairutdinov, R. F. (2000) in *Electron Transfer in Chemistry* (Balzani, V., Ed.) Vol. 4, Wiley-VCH, Weinheim, Germany (in press).
50. Tachiya, M. (1987) in *Kinetics of Nonhomogeneous Processes* (Freeman, G. R., Ed.) pp 575−612, Wiley, New York.
51. Lymar, S. V., and Hurst, J. K. (1994) *J. Phys. Chem. 98*, 989−996.
52. Gennis, R. B. (1989) *Biomembranes-Molecular Structure and Function*, Springer-Verlag, New York.
53. Soszynski, M., and Bartosz, G. (1996) *Biochim. Biophys. Acta 1291*, 107−114.
54. Gadelha, F. R., Thomson, L., Fagian, M. M., Costa, A. D. T., Radi, R., and Vercesi, A. E. (1997) *Arch. Biochem. Biophys. 345*, 243−250.
55. Radi, R., Beckman, J. S., Bush, K. M., and Freeman, B. A. (1991) *Arch. Biochem. Biophys. 288*, 481−487.
56. Bauer, M. L., Beckman, J. S., Bridges, R. J., Fuller, C. M., and Matalon, S. (1992) *Biochim. Biophys. Acta 1104*, 87−94.
57. Mallozzi, C., Michela di Stasi, M., and Minetti, M. (1997) *FASEB J. 11*, 1281−1290.
58. Viner, R. I., Williams, T. D., and Schöneich, C. (1999) *Biochemistry 38*, 12408−12415.
59. Hunt, J. A., Lee, J., and Groves, J. T. (1997) *Chem. Biol. 4*, 845−858.
60. Lymar, S. V., and Hurst, J. K. (1995) *Chem. Res. Toxicol. 8*, 833−840.
61. Lilie, J., Hanrahan, R. J., and Henglein, A. (1978) *Radiat. Phys. Chem. 11*, 225−227.
62. Gratzel, M., Henglein, A., Lilie, J., and Beck, G. (1969) *Ber. Bunsen-Ges. Phys. Chem. 73*, 646−653.
63. Goldstein, S., and Czapski, G. (1995) *J. Am. Chem. Soc. 117*, 12078−12084.

64. Huie, R. E., Shoute, L. C. T., and Neta, P. (1991) *Int. J. Chem. Kinet. 23*, 541−552.
65. Elliot, A. J., McCracken, D. R., Buxton, G. V., and Wood, N. D. (1990) *J. Chem. Soc., Faraday Trans. 86*, 1539−1547.
66. Holcman, J., Bjergbakke, E., and Sehested, K. (1987) *Proc. Tihany Symp. Radiat. Chem. 6*, 149−153.
67. Czapski, G., Holcman, J., and Bielski, B. H. J. (1994) *J. Am. Chem. Soc. 116*, 11465−11469.
68. Buxton, J. V., Greenstock, C. L., Helman, W. P., and Ross, A. B. (1988) *J. Phys. Chem. Ref. Data 17*, 513−886.

BI001270X